IEEE Access
Multidisciplinary | Rapid Review | Open Access Journal

Received March 19, 2020, accepted April 1, 2020, date of publication April 6, 2020, date of current version April 22, 2020.

Digital Object Identifier 10.1109/ACCESS.2020.2985845

A Gap Coupled Hexagonal Split Ring Resonator Based Metamaterial for S-Band and X-Band Microwave Applications

MOHAMMAD SHAHIDUL ISLAM[1], (Student Member, IEEE), MD. SAMSUZZAMAN[1], (Member, IEEE), GAN KOK BENG[1], NORBAHIAH MISRAN[1], NOWSHAD AMIN[2], AND MOHAMMAD TARIQUL ISLAM[1], (Senior Member, IEEE)

[1]Department of Electrical, Electronic, and Systems Engineering, Universiti Kebangsaan Malaysia, Bangi 43600, Malaysia
[2]Institute of Sustainable Energy, Universiti Tenaga Nasional (The National Energy University), Selangor 43000, Malaysia

Corresponding authors: Mohammad Shahidul Islam (P97645@siswa.ukm.edu.my), Md. Samsuzzaman (samsuzzaman@ukm.edu.my), and Mohammad Tariqul Islam (tariqul@ukm.edu.my)

This work was supported by the University Research Grant DIP-2018-018 of Universiti Kebangsaan Malaysia.

ABSTRACT A gap coupled hexagonal split ring resonator (GCHSRR) based metamaterial is presented in this paper for S-band and X-band microwave applications with absorptance. This gap coupled hexagonal split ring resonator is the amendment of the typical split-ring resonator (SRR). Three interconnected hexagonal split ring resonators are applied with a stripline to increase the electrical length and coupling effect of the GCHSRR. SRR has an impact on the extraction of effective parameters such as permittivity, permeability and refractive index. The dimension of the proposed GCHSRR unit cell is 10×10 mm^{2,} which is printed on low-cost FR4 material. The transmission frequency of the proposed GCHSRR unit cell ranges from 3.42 GHz to 3.73 GHz and 11.27 GHz to 11.91 GHz, which makes the metamaterial applicable for S-band and X-band microwave applications. The GCHSRR unit cell has a double negative regime of 7.92 GHz to 9.78 GHz with an effective negative refractive index regime of 6.30 GHz to 10.22 GHz and 11.97 GHz to 12.61 GHz. The effective medium ratio is 8.4, which implies the novelty of the proposed design. Moreover, the GCHSRR has high absorption peaks of 99%, 98%, and 81% at 4.27 GHz, 5.42 GHz, and 12.40 GHz, respectively. An 18×20 GCHSRR array structure is also designed and studied. The effective parameters and the effective medium ratio with a high absorptance make the proposed GCHSRR based metamaterial suitable for practical microwave applications.

INDEX TERMS Split ring resonator, metamaterial, absorptance, effective medium ratio.

I. INTRODUCTION

Wave-matter interactions like X-ray diffraction, infra-red spectroscopy or magnetic resonance lead to the advent of a new area of artificial media, which is called metamaterials. The metamaterial is the artificially engineered object that is organized on scale of operating wavelength, and that induces a new macroscopic characteristic by interacting with the waves. Taming magneto-optical nonreciprocal phenomena and tailoring the light wave dispersion is the unique way that might be provided by the metamaterials [1], [2]. Metamaterials that can provide unique properties such as electrical and magnetic resonance, negative refractive index, cloaking, etc., are called left-handed materials (LHM). LHM can be categorized as double negative metamaterials (DNG) and single negative metamaterials (SNG), often formed by the split ring resonators (SRR) [3], [4] and embedded conducting thin wires for a specific frequency range. DNG has unique properties of negative refractive index including both negative permittivity and permeability where single negative metamaterial has either negative permittivity or negative permeability accompanied by constant evanescent wave propagation [5], [6]. For displaying the basic resonant mode, SRR is the key component where the resonant frequency is

The associate editor coordinating the review of this manuscript and approving it for publication was Lin Peng.

determined by its geometrical structure that leads to microwave and millimeter frequency regimes with electric permittivity and magnetic permeability [7], [8]. A new form of single negative metamaterial has been developed and investigated to demonstrate the negative effective parameter behavior in the microwave and millimeter frequency range for sensing applications [5]. For electromagnetic shielding, a compact meander line elliptic split ring resonator based metamaterial is designed and developed at [9]. This paper analyzes the actual absorption and concludes the acceptability as an ideal candidate in WiMAX, the WLAN industry for microwave applications. A tri-band metamaterial unit cell has been designed and developed at [10] where the absorption efficiency with the operating bandwidth in C, X, and Ku-band has explicated. Electromagnetic (EM) wave absorber absorbs EM energy as a functional material. The metamaterial absorber is a new kind of EM absorber that is composed of electrically small units. These metamaterial absorbers are convenient for wireless communication systems like cognitive radio networks, intelligent radar systems, etc [11]. A metamaterial absorber for X-band is presented at [12], where the results show 75% absorption. Ultra-broadband metamaterial absorber is presented at [13], where the initial absorption 75% that has further been pushed to 92% absorption efficiency in the microwave region. A triple band ultrathin metamaterial has been proposed at [14] where the absorption peaks are at 3.25 GHz, 9.45 GHz and 10.90 GHz with above 90% absorption. This structure has the wide angle and polarization stability that can be used in C-band and Ku-band applications. Various extensive research has also been performed in terahertz region for the multiband metamaterial absorber. A thin frequency selective surface based on rectangular SRR has been proposed at [15] where the metamaterial is composed of subwavelength electromagnetic structures which operates at X-band and Ku-band. This structure has usage in antireflection coatings, sensors and radiators. As compactness of the metamaterial is an important issue, effective medium ratio (EMR) has been described as the solution where it indicates the ratio of the wavelength and the dimension of the metamaterial unit cell. A resonator-based metamaterial for microstrip technology with EMR 4.76 is explained at [16], where it covers the L-band. A new composite metamaterial for multi-band communication with an EMR of 7.44 is described at [17].

In this paper, a gap coupled with hexagonal split ring resonator (GCHSRR) based metamaterial has been proposed for S-band and X-band microwave applications. DNG region has been found from 7.92 GHz to 9.78 GHz with effective negative refractive index region of 6.30 GHz to 10.22 GHz and 11.97GHz to 12.61 GHz. The assessment of the proposed unit cell structure's negative index properties, compactness and bandwidth are evaluated by EM wave propagation. The proposed GCHSRR unit cell's effective medium ratio is 8.4 that defines the compactness and acceptability. However, the effective absorption peaks are 99%, 98%, and 81% for 4.27 GHz, 5.42 GHz, and 12.40 GHz, respectively. In addition, GCHSRR unit cell and its array structure of 1×1 and 2×2 unit cell have been analyzed in order to check the similarity with the identified effective parameters. The proposed GCHSRR unit cell exhibits the single and DNG characteristics at S-band and X-band, respectively. To validate the performance of the simulated and measured results of the proposed GCHSRR unit cell and it 18×20 unit cell array structure, waveguide ports and horn antennas have been used to measure which shows a good agreement among the results.

II. DESIGN PROCEDURE OF UNIT CELL STRUCTURE

A gap coupled hexagonal split-ring resonator (GCHSRR) metamaterial unit cell is presented in Figure 1. SRR is one of the widely applied artificial magnetic materials [18], and it consists of circular, rectangular, spiral, omega, etc. metallic rings, which are printed in a dielectric medium. Each of the forms has its coupling effect based on its shape, and electromagnetic properties such as circular shape have edge coupling effect, rectangular shape has broadside coupling effect, etc. In addition, a single split ring resonator possesses bianisotropic responses, and cross-polarization effects as electric field excite the magnetic dipole moment. These bianisotropic behavior and cross-polarization effects are eliminated if there is any broadside nature of the metallic rings [19]–[21]. Thus, the hexagonal shaped SRR has been proposed. As it has broadside nature in its shape, it can eliminate the bianisotropic responses and cross-polarization effects in the dielectric medium. Another reason to choose hexagonal shape is that additional capacitive loading is created in this structure with achieving stronger resonance behavior. Furthermore, significant miniaturization factors [22], [23] can also be achieved by this proposed hexagonal-shaped SRR. The dielectric substrate material is FR4, where the dielectric constant is 4.4, thickness is 1.6mm, and loss tangent

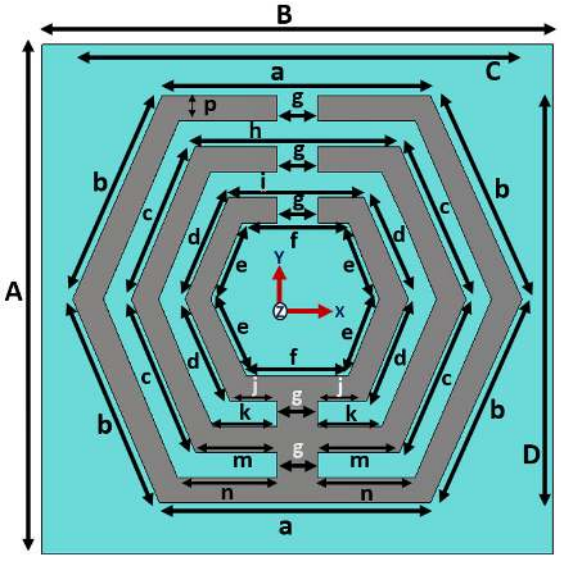

FIGURE 1. The geometric configuration of the unit cell.

is 0.02, respectively. The thickness of the metal in SRR is 0.035 mm, and it is accountable to fix the resonance frequency with capacitance and inductance. The copper-based ring resonator is printed on the FR4 substrate material creates electromagnetic radiation and matches the impedance. Frequency domain-based EM simulator software CST is applied to design and analyze the properties of the proposed GCHSRR unit cell. The design specifications of the proposed GCHSRR metamaterial unit cell structure is illustrated in Table 1.

TABLE 1. Parameters of proposed unit cell.

Substrate Length A	Patch Length C	a	b	c	d	e	f	n
10.0 mm	8.00 mm	5.30 mm	4.39 mm	3.25 mm	2.19 mm	1.62 mm	2.10 mm	1.95 mm
Substrate Width B	**Patch Width D**	**g**	**h**	**i**	**j**	**k**	**m**	**p**
10.0 mm	8.80 mm	0.80 mm	4.00 mm	2.64 mm	0.92 mm	1.25 mm	1.60 mm	0.50 mm

The step-by-step design mechanism of the proposed GCHSRR metamaterial unit cell with the scattering parameters has been analyzed through the design mechanism. Figure 2 (a) and Figure 2 (b) represents the reflection and transmission coefficient of different splits, from single split to multiple splits and their connections. It is noticeable that the proposed GCHSRR unit cell has the maximum resonance in frequency bands with good scattering values.

III. EFFECTIVE MEDIUM PARAMETERS AND MEASUREMENT TECHNIQUE

The frequency domain-based EM simulator software CST microwave studio is used to calculate the effective medium parameters of the proposed GCHSRR unit cell and its unit cell array structures where the unit cell and array structure are placed in between positive Z-axis and negative Z-axis waveguide ports and energized towards the Z-axis by the electro-magnetic wave shown in Figure 3. To get the ideal electromagnetic field, the direction has been set in X-axis and Y-axis for the boundary conditions. An electric field is tangent to the inclusions, and magnetic field is normal to the surface structure where these characteristics direct the metamaterial's responses. The PEC boundary conditions has been applied in two ways, (i) perpendicular to the electric vector with upper and lower side of GCHSRR unit cell, and (ii) perpendicular to the magnetic vector with back and front side of GCHSRR unit cell.

The open add boundary has been used for operating in the free space. A distance of $2D^2/\lambda$ (D: diameter of the antenna and λ: free space wavelength) is used to extend the open add space boundary condition, which helps to investigate the electric field in the near field region. Therefore, it is possible to examine the field characteristics of resonant frequencies by incorporating different fields such as electric, magnetic

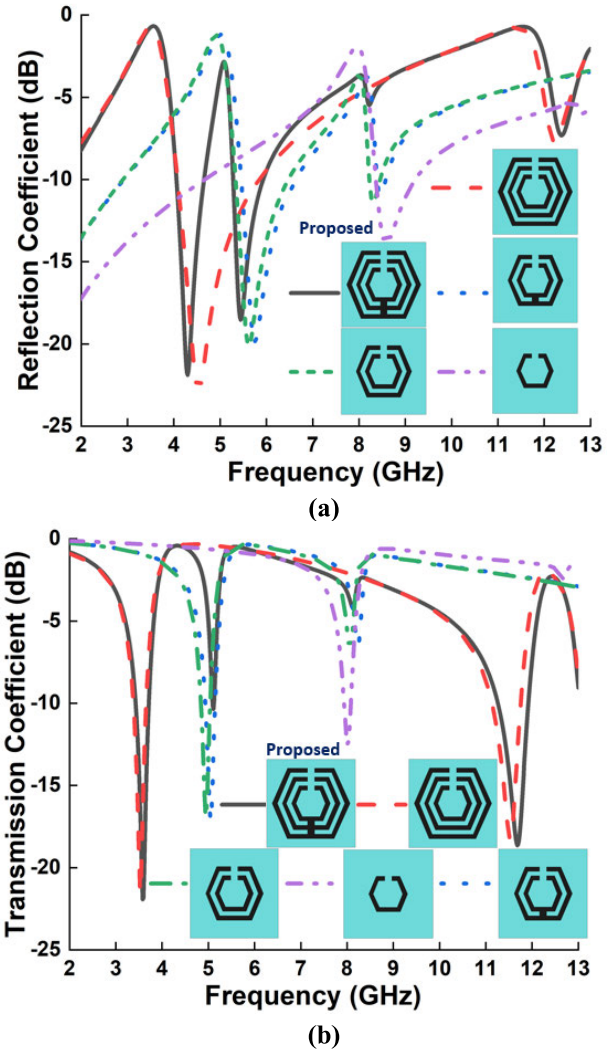

FIGURE 2. (a) Reflection coefficient and (b) transmission coefficient analysis.

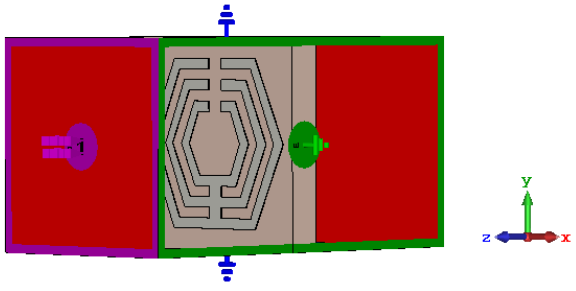

FIGURE 3. The boundary condition of the proposed GCHSRR unit cell structure for simulation.

and open space at each wall. Frequency-domain solver with tetrahedral mesh is adopted to simulate the unit cell and array structures from 2 GHz to 13 GHz with a 50-ohm set impedance.

Nicolson-Ross-Weir (NRW) method is one of the most popular methods in electromagnetic characterization of the

metamaterials based on the reflection and transmission measurements of the specimen under test. The impedance and wave velocities are the parameters to retrieve the properties of the metamaterials. NRW method has been used to extract effective medium parameters from the usual incidences of scattering parameter data [24]. The NRW method starts with the implementation of the composite terms V1 and V2, where the scattering parameters are added and subtracted.

$$V_1 = S_{21} + S_{11} \tag{1}$$
$$V_2 = S_{21} - S_{11} \tag{2}$$
$$T = X \pm \sqrt{X^2 - 1} \tag{3}$$

T represents the Interface Reflection Coefficient. The scattering parameters S_{11} and S_{21} of the unit cell can be calculated as follows to extract the effective parameters. , , and represent the permittivity, permeability and refractive index respectively. k_0 and d represent the wave number and thickness of the substrate.

$$S_{11} = \frac{(1 - Z^2)T}{1 - T^2Z^2} \tag{4}$$
$$S_{21} = \frac{(1 - T^2)Z}{1 - T^2Z^2} \tag{5}$$
$$\varepsilon_r = \frac{2}{jk_0d}\frac{1 - S_{21} + S_{11}}{1 + S_{21} - S_{11}} \tag{6}$$
$$\mu_r = \frac{j2S_{11}}{jk_0d} + \mu_0 \tag{7}$$
$$\eta_r = \frac{2}{jk_0d}\sqrt{\frac{(S_{21} - 1)^2 - S_{11}^2}{(S_{21} + 1)^2 - S_{11}^2}} \tag{8}$$

An Agilent N5227 Vector Network Analyzer (VNA) connected with waveguide ports to co-axial adapters have been used to measure the scattering parameters (reflection and transmission coefficient) of the proposed GCHSRR unit cell structure. Waveguides have been used for the frequency ranges of 3.42-3.73 GHz and 11.27-11.91 GHz, respectively. The electromagnetic waves scatter along the z-directions as the proposed unit cell is placed in between different waveguide port, which is shown in Figure 4. The Agilent N4694-60001 calibration kit is used to calibrate the VNA for measurement accuracy.

IV. EQUIVALENT CIRCUIT MODEL

The approximated equivalent circuit representation of the proposed unit cell is shown in Figure 5(a). The Transmission line formula has been used to form the proposed GCHSRR unit cell as, where a series of RLC circuit is reflected by a single patch. This is called the passive LC circuit that interacts with the resonance frequency.

The following equation refers to the relation between the resonance frequency and LC circuit [2],

$$f = \frac{1}{2\pi\sqrt{LC}} \tag{9}$$

L and C are lumped inductance and capacitance. The split within the metal loop indicates capacitance and inductance.

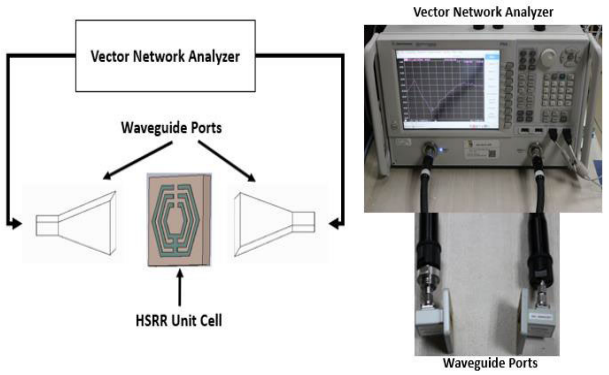

FIGURE 4. Experimental setup for S-parameters measurement of GCHSSR Unit Cell.

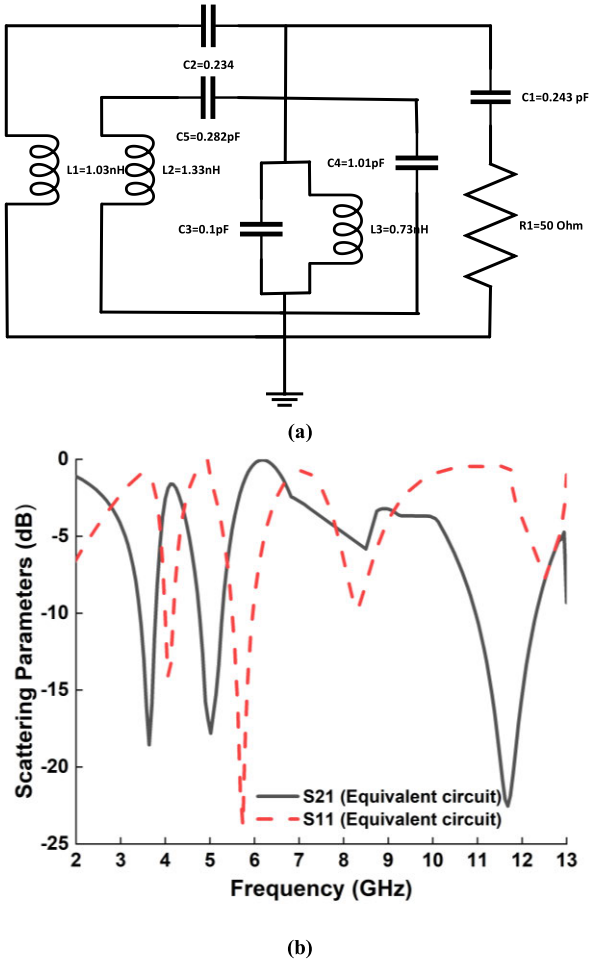

FIGURE 5. (a) Equivalent circuit of GCHSRR Unit Cell and (b) reflection and transmission coefficient of the proposed GCHSRR unit cell equivalent circuit.

Splits and electric field combinedly forms the electric resonance where magnetic fields and magnetic loops combinedly form the magnetic resonance. Both situations happen when the EM wave propagates within the structure. The following formula represents the capacitance.

$$C = \varepsilon_0\varepsilon_r\frac{A}{d}(F) \tag{10}$$

ε_0 presents free space permittivity, ε_r presents relative permittivity. A presents the area of the splits and d presents the split length. The equivalent inductance is determined in accordance with the concept of the transmission line principle described in [2].

$$L(nH) = 2\times10^{-4} l[\ln(\frac{l}{w+t})+1.193+0.02235\frac{w+t}{l}]K_g \tag{11}$$

where l, w and t are the length, width and thickness of microstrip line, correction factor, Kg is $0.57\text{-}0.145ln\frac{w'}{h'}$, where w' and h' represents the width and thickness of the substrate. There must be an evaluation of internal and external inductance to assess the maximum inductance.

Since the reflection coefficient (S_{11}) shows that there are multiple resonance frequencies, so field distribution and surface current form major impact with respect to the equivalent circuit. Initially, Equation 10 and Equation 11 have been used to calculate the L and C magnitudes of the designed circuit. After that the approximated unit cell circuit with calculated values was designed in electromagnetic simulation software ADS for extracting the scattering parameter values. Finally, the optimized values of L and C were achieved which is shown in Figure 5(a). The scattering parameter results of the proposed GCHSRR unit cell equivalent circuit model present in Figure 5(b). C1 to C4 capacitance is the dominating resonance component. Each hexagonal shape microstrip patch arm similar to series RLC circuit and connected through common node showing single resistor and inductor. Both electric and magnetic field have the approximately similar field distribution with some variation in TEM propagation. However, in H-field at that instant, a strong magnetic field exists while forming orthogonal propagation of wave. Hence, this unit cell shows multiple resonance frequencies with good scattering parametric values.

V. ELECTROMAGNETIC FIELD AND SURFACE CURRENT DISTRIBUTION ANALYSIS

The electric field for 11.67 GHz and 3.56 GHz is shown in Figure 6, where the electric field represents the current density. The electric field is higher at the outer hexagonal structure for 11.67GHz where it is lower in the outer hexagonal structure for 3.56GHz. The capacitance and electric resonance are generated due to the splits of the proposed shape. The magnetic field for 11.67 GHz and 3.56 GHz is shown in Figure 7. It is noted that there must be opposite excitation between the electrical field and the magnetic field. The electric field and the magnetic field show the opposite excitation for both 3.56 GHz and 11.67 GHz that meets the Maxwell equation criterion. The excitation in the surface current distribution for 3.56 GHz and 11.67 GHz is shown in Figure 8 where the intensity of the currents is expressed by different colors. The inner surface of the hexagonal resonator has the lesser current intensity compared to the outer surface of the hexagonal structure. It is noticeable that the outer hexagonal resonator contains stronger current intensity for 11.67 GHz compare to the outer hexagonal resonator for 3.56 GHz.

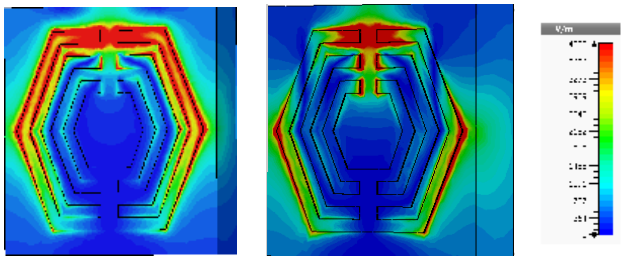

FIGURE 6. Electric Field at 3.56 GHz and 11.67 GHz, Respectively.

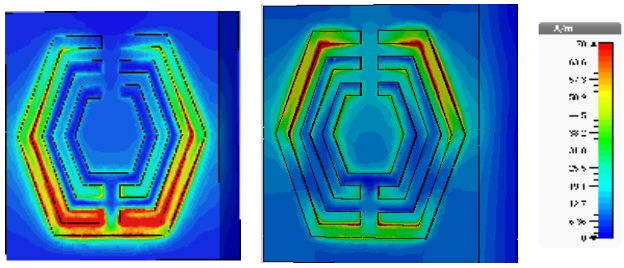

FIGURE 7. Magnetic Field at 3.56 GHz and 11.67 GHz, Respectively.

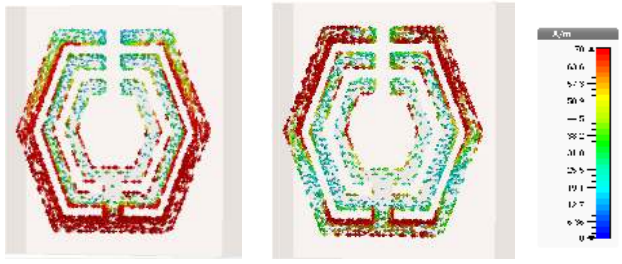

FIGURE 8. Surface Current at 3.56 GHz and 11.67 GHz, Respectively.

DNG metamaterial characterized by two complex constitutive parameters named permittivity (ε) and permeability (μ). The relations within their real and imaginary part are given in Equation 12 and Equation 13. ε' and μ': Real part, ε'' and μ'': Imaginary part,

$$\varepsilon = \varepsilon' + i\varepsilon'' \tag{12}$$

$$\mu = \mu' + i\mu'' \tag{13}$$

Equation 14 and Equation 15 represents the Maxwell's equations on left hand rule in the differential form,

$$\nabla \times E = -\frac{\partial B}{\partial t} \tag{14}$$

$$\nabla \times H = \frac{\partial D}{\partial t} \tag{15}$$

and the two constitutive relations to the applied fields, μ_0

$$B = \mu_0 \mu H \tag{16}$$

$$D = \varepsilon_0 \varepsilon E \tag{17}$$

DPS medium does not exhibits non-standard electromagnetic effects of reflection and refraction of the backward waves whereas it only exists in the DPS-DNG medium interface. The propagation of electromagnetic waves in any complex structure contains both DNG and DPS media. Figure 9 represents the DPS- DNG slabs where artificial, lossy DNG slab is placed between two natural, lossy DPS slabs of Air substrate that are analyzed through electromagnetic wave propagation. The dimension of the DPS slabs is the same as the proposed GCHSRR unit cell, and it contains the constitutive parameters of $\boldsymbol{\varepsilon} = \mathbf{1}$ and $\boldsymbol{\mu} = \mathbf{1}$.

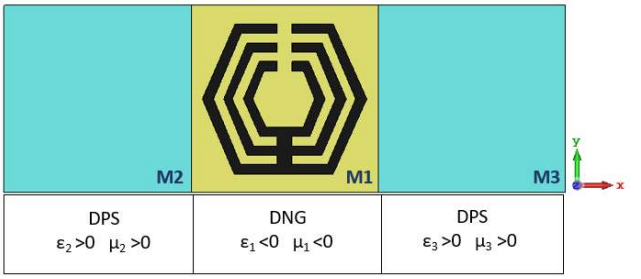

FIGURE 9. DPS-DNG-DPS slab.

The electric and magnetic field intensity distribution for the DNG media are captured and compared against the reference case of two DSP slabs shown in Figure 10. Negative refracted waves in the DNG slabs and backward wave propagation have been an observing fact. As the permittivity and permeability are negative, the electromagnetic wave propagation inside the DNG medium is permissible.

VI. PARAMETRIC ANALYSIS OF THE PROPOSED GCHSRR UNIT CELL STRUCTURE

Effective medium parameters with electromagnetic characteristics have been extracted from the NRW method and direct refractive index method (DRI). The parametric analysis of the proposed GCHSRR unit cell and its unit cell array structure has also been performed in this study. Scattering parameters such as the reflection coefficient and transmission coefficient have been analyzed through the parametric studies of the proposed GCHSRR unit cell. The analysis has been performed based on connecting the gaps between the splits. It is noticeable that the proposed structure covers the maximum bands with multiple resonance frequencies for both reflection and transmission coefficient which is shown as Figure 11. The short-range coupling in metamaterial occurs due to the nearest resonators. The gaps of the SRR does the electric field coupling and the circumference does the magnetic field coupling depending on the near field characteristics. In Figure 12 (a), MM1 is the 1 × 2 array structure. MM2 and MM3 are symmetrical with facing each other. Besides, MM4 has asymmetrical coupling. In terms of decreasing the distance, there has been a significant change in the transmission coefficient which is shown in Figure 12 (b). The resonance has been shifted, and only one transmission

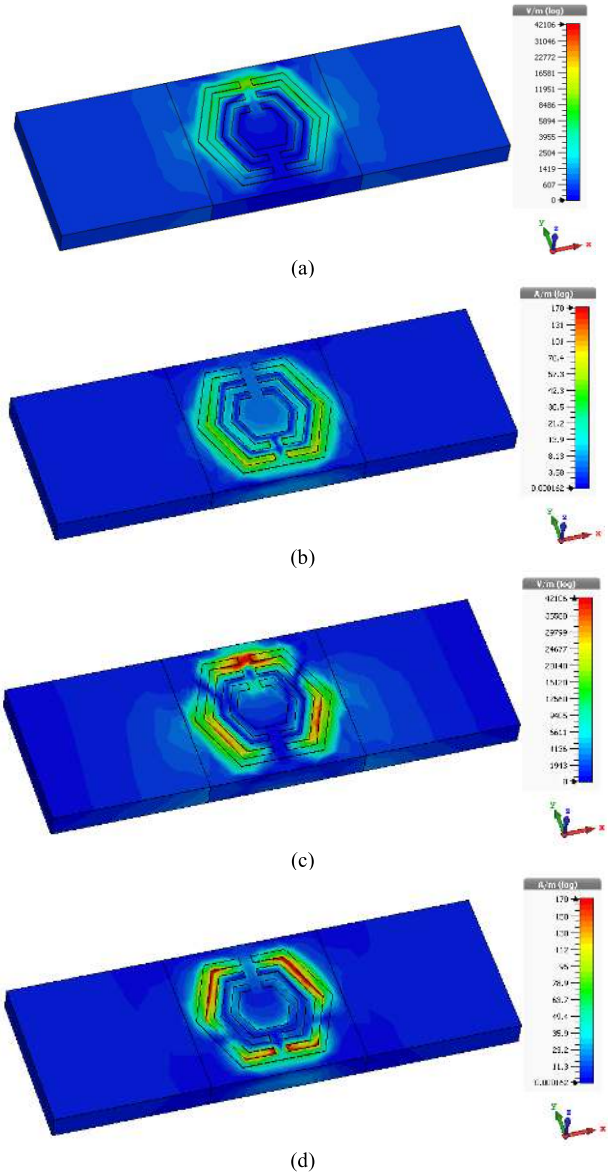

FIGURE 10. Electromagnetic wave interaction within DNG medium (a) E-Field at 3.56 GHz (b) H-Field at 3.56 GHz (c) E-Field at 11.67 GHz (d) H-Field at 11.67 GHz.

frequency arises at the higher frequency zone. 2 × 2 structures have been analyzed where MM5 is asymmetrical, and MM6 and MM7 are symmetrical, facing each other in different phases. The resonances have been changed for MM5 and MM6 with one transmission frequency. For MM7, the resonance frequency has slightly been shifted. It is noticeable that the symmetric and asymmetric positions of the 1 × 2 and 2 × 2 structures facing each other have strong coupling effect causing frequency shifts. In addition, the symmetric gap position in 1 × 2 structure has a weak coupling effect causing slight frequency shifts.

Figure 13 shows the proposed GCHSRR unit cell with boundaries. The effective frequency has been set from 2 GHz to 13 GHz to calculate the effective parameters. The extracted

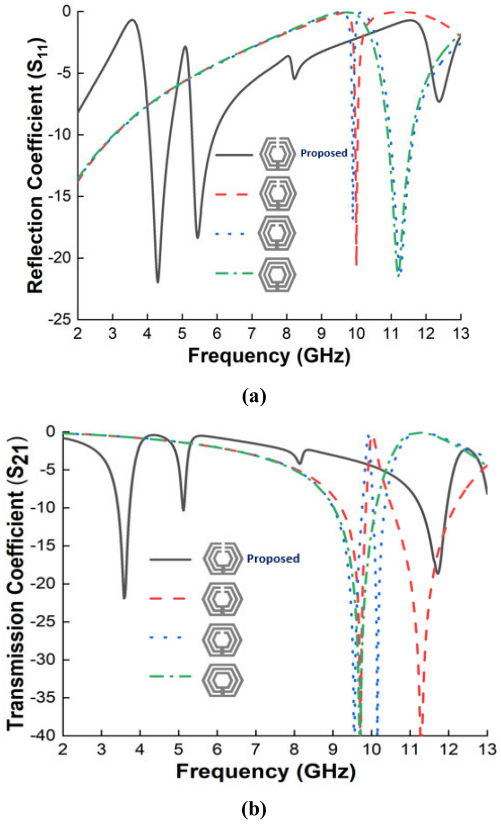

FIGURE 11. Parametric analysis of different unit cell structure (a) S_{11} (b) S_{21}i.

real and imaginary scattering parameters S_{11}, S_{21}, effective permittivity, permeability, and refractive index are shown in Figure 14 (a-e). Table 2 represents the frequency regimes of negative permittivity, permeability, refractive index, and double-negative regions. The double negative region for the proposed structure ranges from 7.92 GHz to 9.78 GHz. Table 3 represents the frequency regimes of negative permittivity, permeability, refractive index, and double-negative regions. The DNG region for the proposed 1 × 2 array structure ranges from 7.96 GHz to 9.57 GHz and 12 GHz to 12.71 GHz, respectively. Table 4 represents the frequency regimes of negative permittivity, permeability, refractive index, and double-negative regions. The double negative region for the proposed 2 × 2 array structure ranges from 11.96 GHz to 12.87 GHz.

VII. ABSORPTION OF GCHSRR UNIT CELL AND ARRAY STRUCTURE

Electromagnetic wave absorber absorbs EM energy, and it is mainly realized by high electric loss materials. The metamaterial can work as EM absorber, which is normally composed of arranged electrically small unit cells in a two-dimensional plane.

Because of the electric and magnetic resonance in the metamaterial, the impedance matches in free space with

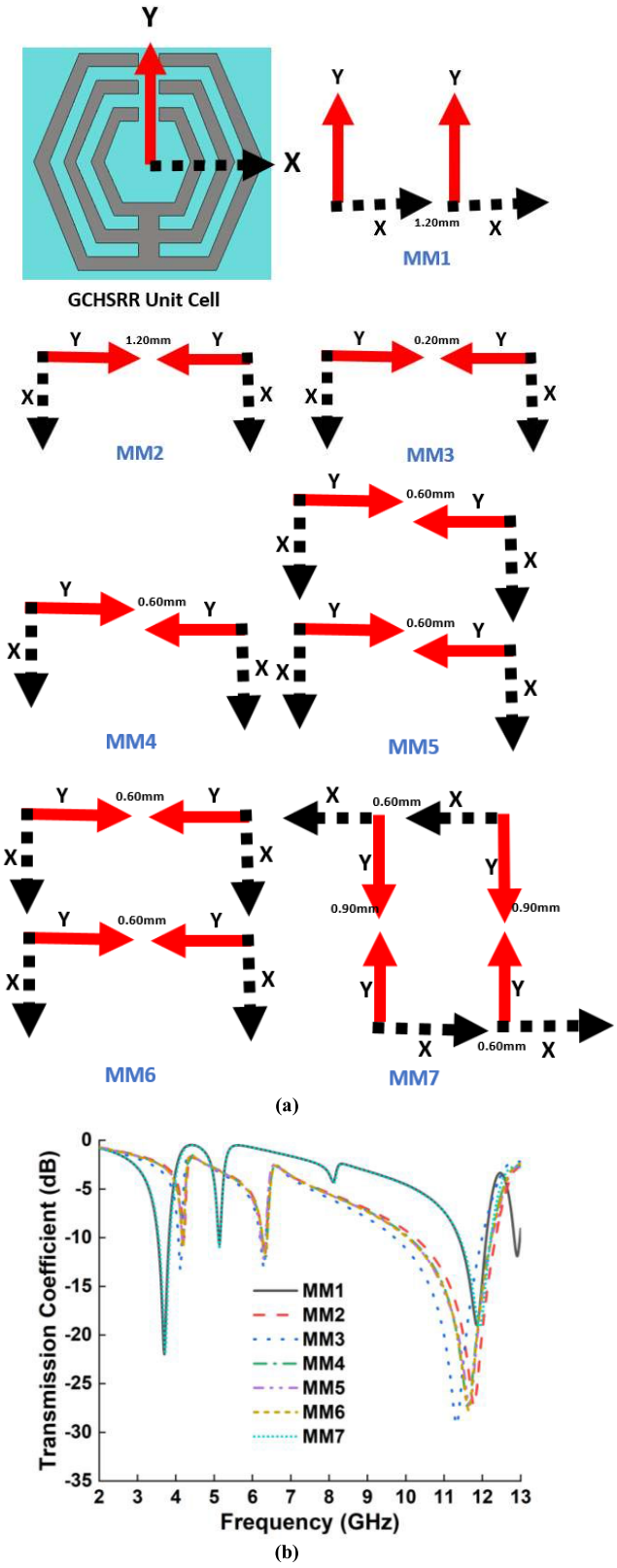

FIGURE 12. (a) Coupling effects and (b) transmission coefficient on symmetric and asymmetric structure for 1 × 2 and 2 × 2 array structure.

effective permittivity and permeability. Thus, there does not occur any reflection in the interface, and the entire incident energy is absorbed in the metamaterial absorber.

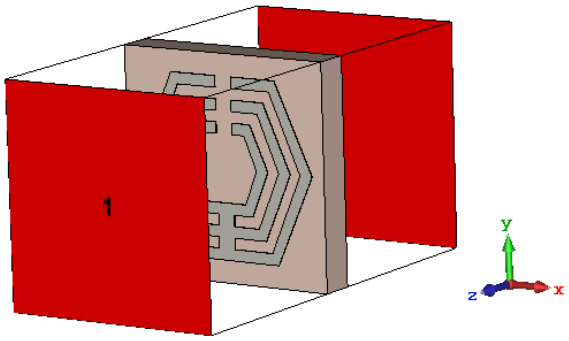

FIGURE 13. Proposed GCHSRR Unit Cell.

TABLE 2. Negative effective parameters frequency region of the proposed GCHSRR unit cell.

Parameters	The frequency range of negative index in GHz
Effective Permittivity	3.23-3.78, 4.87-5.15, 6.00-9.78
Effective Permeability	7.92-12.76
Effective Refractive Index	6.30-10.22, 11.97-12.61
Double Negative Region	7.92-9.78

TABLE 3. Frequency region of negative effective parameters of 1 × 2 GCHSRR unit cell.

Parameters	The frequency range of negative index in GHz
Effective Permittivity	3.16-3.83, 4.83-5.15, 5.96-9.57, 12-12.71
Effective Permeability	7.96-12.76
Effective Refractive Index	6.09-10.12, 11.05-12.72
Double Negative Region	7.96-9.57, 12-12.71

TABLE 4. Frequency region of negative effective parameters of 2 × 2 GCHSRR unit cell.

Parameters	Frequency range of negative index in GHz
Effective Permittivity	2.99-3.14, 3.38-3.95, 4.83-5.19, 5.83-7.09, 11.96-12.87
Effective Permeability	7.966-12.97
Effective Refractive Index	6.00-7.02, 7.28-9.90, 11.25-12.95
Double Negative Region	11.96-12.87

The absorption can be considered from the following formula [9].

$$Absorption, A = 1 - |S_{11}|^2 - |S_{21}|^2 \tag{18}$$

The absorption of the proposed GCHSRR unit cell, 1 × 2 array, and 2 × 2 array is depicted in Figure 15. Table 5 represents the absorption at different resonance frequency of unit cell, 1 × 2 array and 2 × 2 array structures. The proposed

TABLE 5. Absorption at the resonance frequency.

Parameters	Unit Cell			1×2 Array			2×2 Array		
Resonance of S_{11} (GHz)	4.27	5.42	12.40	4.29	5.43	12.45	4.33	5.44	12.70
Absorption (100%)	99 %	98 %	81%	99 %	98 %	81%	99 %	98 %	86%

TABLE 6. Extracted value of different shapes.

Shape	Resonance Frequency	Real Impedance	Absorption	Absorption Band
1	4.27 GHz 5.42 GHz 12.4 GHz	1.01 Ω 0.95 Ω 1.2 Ω	99% 98% 81%	3
2	3.03 GHz 7.91 GHz	0.33 Ω 1.02 Ω	91% 42%	2
3	3.57 GHz	0.72 Ω	17%	1

GCHSRR unit cell and its array structure 1 × 2 and 2 × 2 have a high absorption of 99% at the resonance of 4.27 GHz, 4.29 GHz, and 4.33 GHz, respectively. For the resonance frequency of 5.42 GHz, 5.43GHz and 5.44 GHz for the unit cell, 1 × 2 and 2 × 2 respectively, the absorption is 98%. The resonance frequency shows slightly different absorption 86% at 12.70 GHz for 2 × 2 array, but the absorption is same 81% for unit cell and 1 × 2 array at 12.40 GHz and 12.45 GHz, individually.

The normalized input impedance (Z) for the proposed GCHSRR is shown in Figure 16, which has been extracted through the following equation.

$$Z = \pm\sqrt{\frac{(1+S_{11})^2 - S_{21}^2}{(1-S_{11})^2 - S_{21}^2}} \tag{19}$$

Absorption in metamaterial can be achieved by eliminating the transmitted waves through the conductive and dielectric losses. The transmission coefficient of the proposed GCHSRR unit cell is nearly zero for the reflection coefficient of 4.27 GHz, 5.42 GHz, and 12.4 GHz. Thus, the transmission is assumed as zero, $|S_{21}| = 0$.

$$Z = \pm\frac{1+S_{11}}{1-S_{11}} \tag{20}$$

Since the absorption frequency band exhibits both negative permittivity and permeability, the propagation constant become positive according to Helmholtz equation where electric and magnetic field, both try to propagate inward direction rather than outward direction [25]. Furthermore, the exciting element in waveguide port has been placed within the close proximity of the patch element, so distributed field tried to

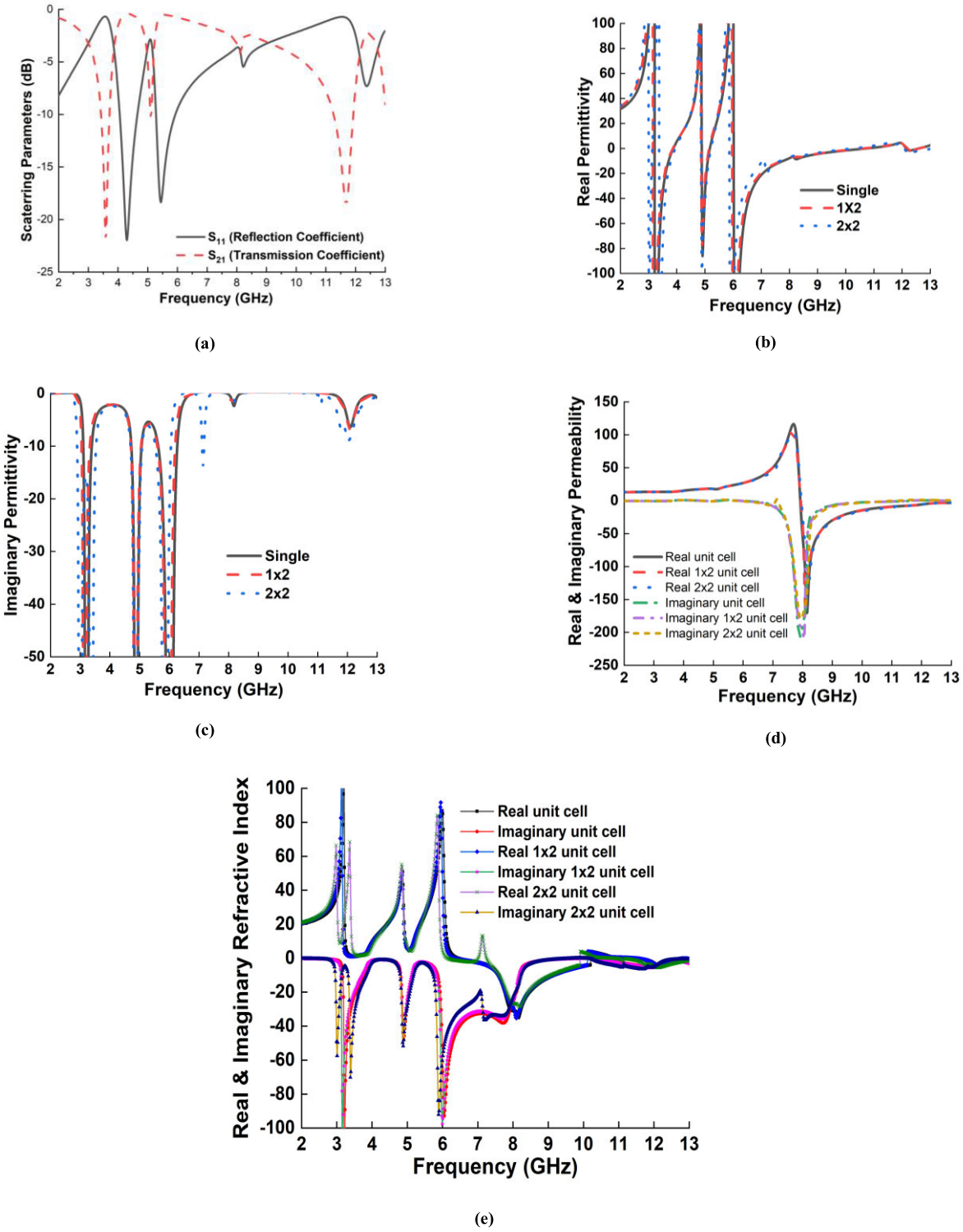

FIGURE 14. (a) Reflection coefficient (S_{11}) & transmission coefficient (S_{21}) of the unit cell (b) real permittivity (c) imaginary permittivity (d-e) real and imaginary permeability, and refractive index, respectively.

absorb by the unit cell itself. Hence, without any back metallic plane the proposed unit cell depicts maximum absorptance on those frequency.

$$\nabla^2 E_m - \gamma^2 E_m = 0 \tag{21}$$
$$\nabla^2 H_m - \gamma^2 H_m = 0 \tag{22}$$

where $E_m$represents the electric field distribution component or propagation, and γrepresents the propagation constant.

$$|\gamma^2| = \omega\mu\sqrt{\sigma^2 + \omega^2\varepsilon^2} \tag{23}$$

The absorption peaks are 99% at 4.27 GHz, 98% at 5.42 GHz, and 81% at 12.4 GHz. The real impedance and imaginary

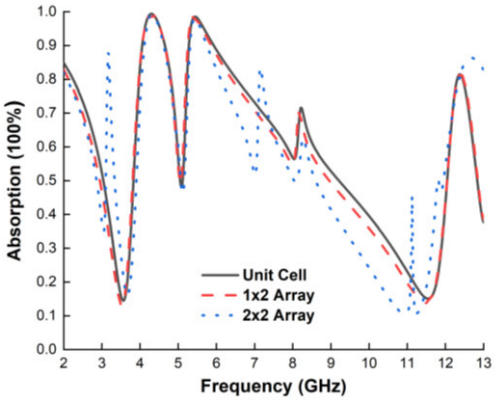

FIGURE 15. Parametric analysis of array structure absorption.

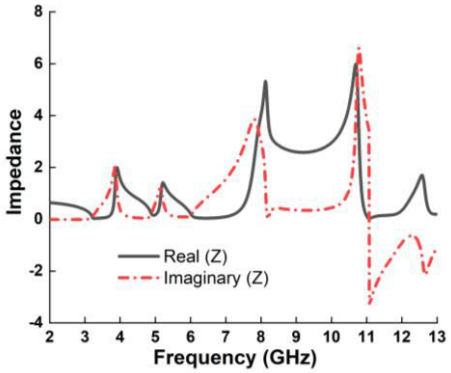

FIGURE 16. Effective Impedance of the Proposed GCHSRR Unit Cell.

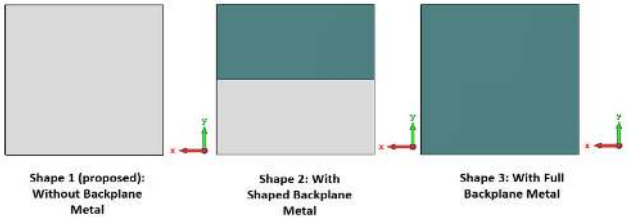

FIGURE 17. Parametric Studies on Backplane of GCHSRR Unit Cell.

impedance are 1.01 Ω and 0.09 Ω, respectively, at 4.27 GHz. At 5.42 GHz, the real impedance is 0.95 Ω, and the imaginary impedance is 0.1 Ω. At 12.4 GHz, the real impedance is 1.2 Ω, and the imaginary impedance is −0.7 Ω. At these absorption peaks, the real parts of the impedance are close to the unity where the imaginary parts are close to zero. This characteristic state that the normalized input impedance matches closely to the free space impedance that supports the absorption phenomenon which can be represented through the equation (24) and equation (25).

$$\mathrm{Re}[\varepsilon_{eff}(f)]_{f=f_0} = \mathrm{Re}[\mu_{eff}(f)]_{f=f_0} \quad (24)$$

$$\mathrm{Im}[\varepsilon_{eff}(f)]_{f=f_0} = \mathrm{Im}[\mu_{eff}(f)]_{f=f_0} \quad (25)$$

Figure 17 represents the different shapes of the backplane of the proposed unit cell where shape 1 is without the back-

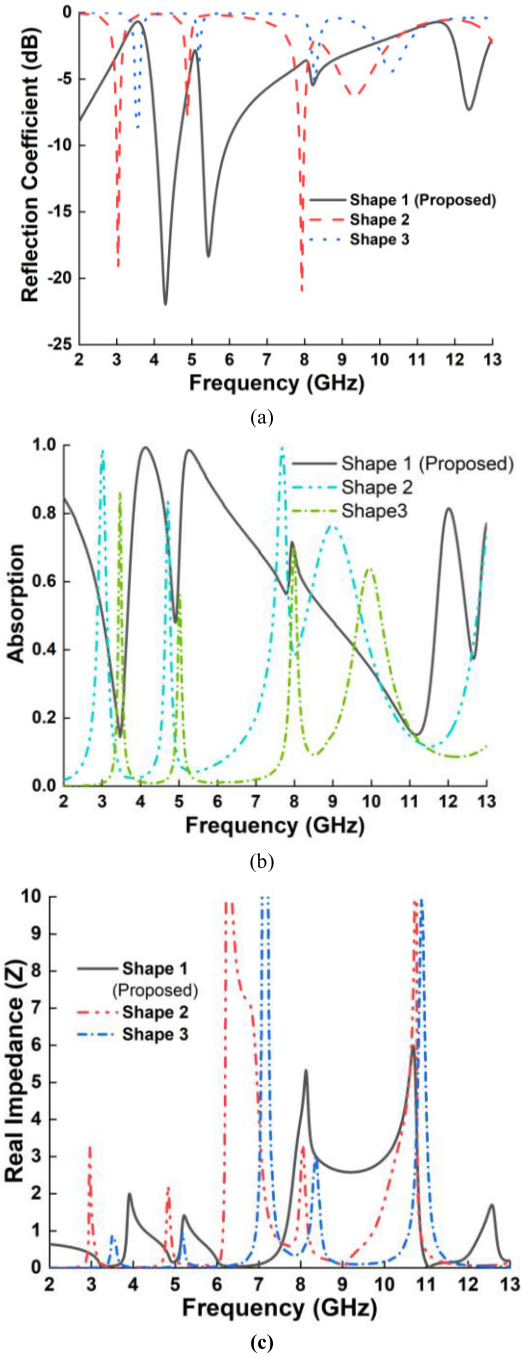

FIGURE 18. Parametric analysis of different shapes with (a) Reflection Coefficient, (b) Absorption and (c) Real Impedance.

plane metal and shape 2 and shape 3 are with the backplane metal. The analysis of real impedance, absorption in terms of reflection coefficient is shown in Figure 18. as well as the values for the resonance peaks are shown in Table 6. The analysis shows that the proposed GCHSRR unit cell has high absorption without the metal backplane compare to other two shapes with metal backplanes. It also has three absorption bands and real impedance that is close to unity. In addition, the comparison among the proposed GCHSRR unit cell and

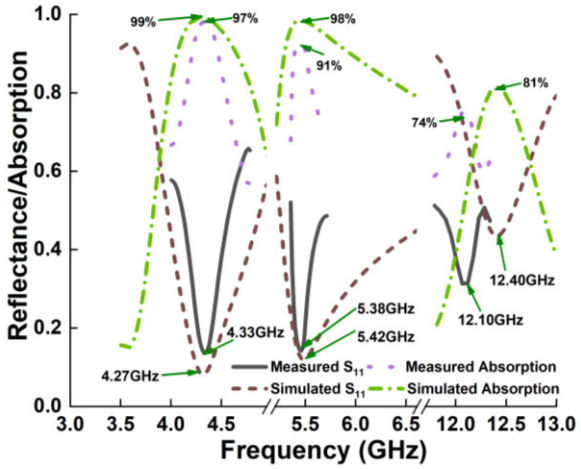

FIGURE 19. Absorption for the simulated and measured reflection coefficient.

existing triple-band absorber are given in Table 7. The absorption has been calculated in terms of simulated and measured reflection coefficient, which is shown in Figure 19.

In simulation result, the resonance peaks are 4.27GHz, 5.42 GHz and 12.40 GHz with 99%, 98%, and 81% absorption, respectively wherein measurement, the resonance peaks are 4.33GHz, 5.38GHz, and 12.10 GHz with 97%, 91%, and 74% absorption, respectively. The 50% absorption bandwidths are 775 MHz, 1.46 GHz and 755 MHz for simulated results and 405 MHz, 220 MHz, and 245 MHz for measured results.

VIII. RESULTS AND DISCUSSION OF GCHSRR UNIT CELL AND ARRAY PROTOTYPE

The measurement arrangement of the proposed unit cell with waveguide ports and (Vector Network Analyzer) VNA is shown as Figure 20 (a-b). Two different waveguides have been used to measure the transmission coefficient that has been found at 3.56 GHz and 11.67 GHz, respectively. The simulated versus measured transmission coefficient has been shown in Figure 20 (c). The frequency range for simulation is from 3.42 GHz to 3.73 GHz whereas frequency range for measurement is from 3.52 GHz to 3.73 GHz. In addition, the other simulated operating frequency ranges from 11.27 GHz to 11.91 GHz whereas the measured frequency ranges from 11.27 GHz to 11.74 GHz. Figure 20 (d) represents the reflection coefficient of simulated versus measured frequency.

Figure 21 (a) represents the fabricated prototype of GCHSRR 18 × 20 array structure. The measurement setup of this array structure is depicted in Figure 21(b). The unit cell array structure is set inside the anechoic chamber. The VNA has been used to measure the reflection and transmission coefficient of the fabricated prototype. An identical copper plate is placed in between of two horn antennas to identify the ideal reflector in the incident wave. Then the fabricated prototype is pace in between the horn antennas for the

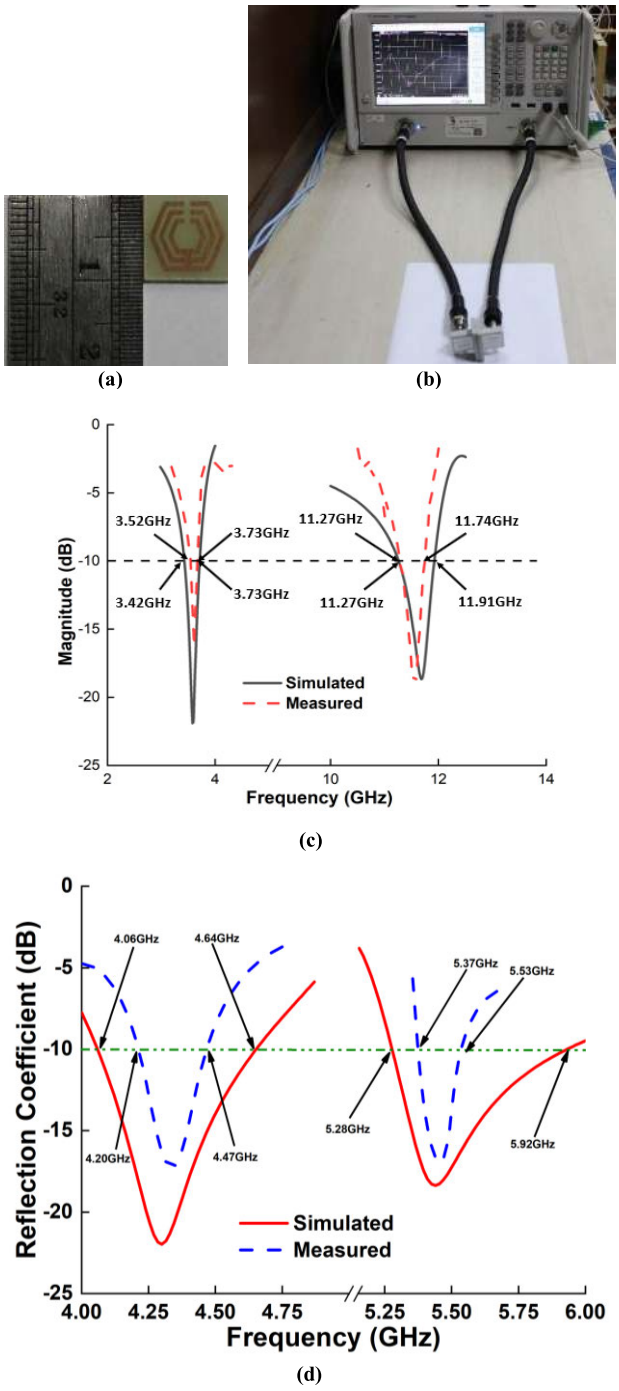

FIGURE 20. (a) Fabricated prototype of GCHSRR unit cell (b) Measurement arrangement of proposed GCHSRR unit cell (c) Simulated and measured magnitude (d) Simulated and measured reflection coefficient.

measurement. The wave propagates towards the z-directions in terms of polarization angle variation (φ), and that is why the normal incidences occur. Figure 21 (c) represents the transmission spectra of the proposed GCHSRR unit cell 18 × 20 array structure.

The frequency ranges from 3.37 GHz to 4.36 GHz and 11.15 GHz to 12.26 GHz, respectively. Good agreement has seen in the simulated and measured result even though there

TABLE 7. Comparison among proposed and existing triple-band absorber.

Reference	Year	Unit Cell Dimension (mm^2)	Substrate	Resonance Frequency (GHz)	Absorption Percentage (%)	Operating Bands/Applications
[26]	2019	11.6×11.6	FR4	8.12 11.40 15.12	96.72 98.28 95.17	Electromagnetic compatibility, stealth technology, and superlenses
[27]	2018	14×14	FR4	3.70 6.57 17.62	99.67 99.05 99.98	Radar stealth, thermal radiometer, spectral imaging
[8]	2019	24×24	FR4	8.60 10.20 11.95	92 84 96	X-Band, Ku-Band
[28]	2019	14×14	FR4	2.90 4.18 9.25	97 96.45 98.20	S-Band, C- Band, X-Band
[29]	2018	10×10	FR4	5.57 7.97 13.44	98.87 97.99 99.28	Defence, explosive detection and airborne radar application
[30]	2018	13.8×13.8	FR4	4.40 6.05 13.90	95.13 97.41 97.36	EM stealth technology, electromagnetic interference, and spectrum identification
[31]	2017	28.2×28.2	FR4	4.20 7.00 7.40	91 98.9 99.5	Air surveillance radar, defence applications
[32]	2017	7.6×7.6	FR4	8.00 10.00 12.00	96 93.36 91.88	X-Band
Proposed	**2019**	**10×10**	**FR4**	**4.27 5.42 12.40**	**99 98 81**	**S-Band, X-Band/ Microwave applications**

TABLE 8. Comparison among the proposed and existing metamaterial unit cell.

Ref.	Unit Cell Shape	Dimensions (mm^2)	Frequency Bands	EMR	Remarks
[33]	Complementary SRR	5.5 × 5.5	C-band	8.0	Extended bands and EMR
[17]	Double C-shaped	12 × 12	S-band, C-band, X-band	7.44	Extended size and EMR
[34]	Modified Z-shaped	10 × 10	X-band	4	Extended bands and EMR
[35]	Modified H-shaped	9 × 9	X-band, Ku-band	3	Extended EMR
[36]	S-shaped	8.5 × 8.5	X-band	2.09	Extended bands and EMR
[37]	S-shaped	10 × 10	X-band	2.4	Extended bands and EMR
[38]	SRR	5 × 5	X-band	6.51	Extended size, bands and EMR
[39]	Circular	5 × 5	X-band	8.45	Extended bands and size
Proposed	**Hexagonal**	**10 × 10**	**S-band, X-band**	**8.4**	**Compact dimension with dual band and more EMR value**

has been a slight shifting in the resonance frequency. This shifting of resonance frequency might occur due to the fabrication error or free space measurement techniques or mutual coupling between the array prototypes, but the prototype still achieves the proposed S-band and X-band, consecutively.

The analysis of GCHSRR unit cell and array structure has been explained in this section. The effective refractive index bandwidth of the proposed unit cell is 3.92 GHz (6.30 GHz to 10.22 GHz) and 640 MHz (11.97 GHz to 12.61 GHz) with a double negative region of 7.92 GHz to 9.78 GHz. This indicates that the proposed unit cell has DNG characteristic at the X-band, which is applicable for satellite and space communication. Although the proposed unit cell has DNG, it also exhibits the single negative characteristics with negative permittivity region of 3.23 GHz to 3.78 GHz which is followed by the transmission coefficient at 3.56 GHz. This characteristic allows the metamaterial to be applicable for microwave device communications.

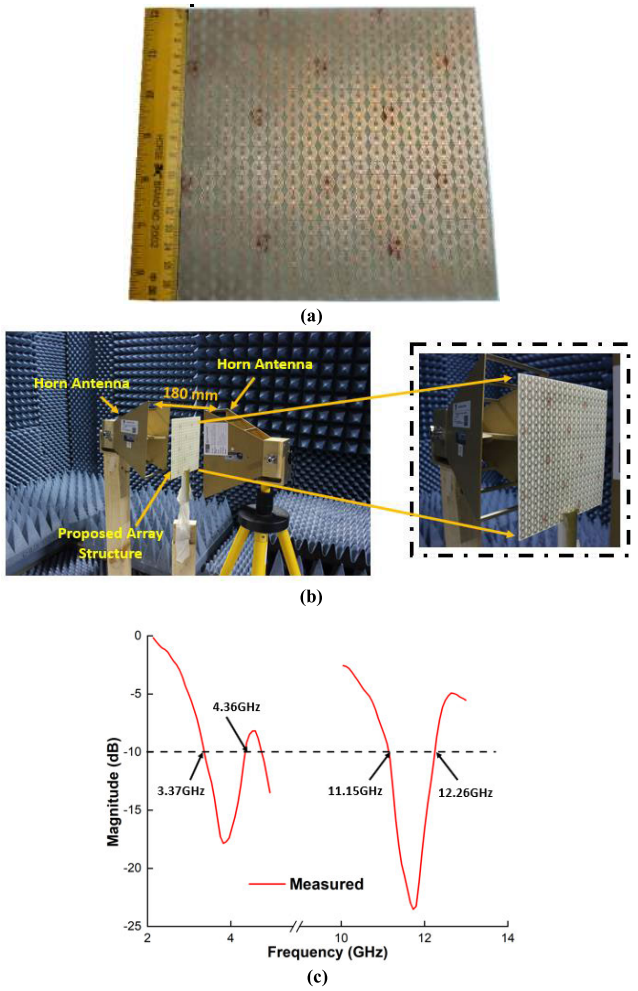

FIGURE 21. (a) Fabricated prototype of GCHSRR 18 × 20 array unit cell structure (b) Measurement of GCHSRR unit cell array structure with horn antenna (c) Measured transmission Spectra of the proposed GCHSRR array structure.

The EMR is an important research area nowadays for the metamaterials which direct the metamaterial compactness. The following calculation has been used to extract the EMR where λ and L represent the wavelength and the dimension, respectively, for the proposed GCHSRR unit cell. The proposed GCHSRR unit cell EMR values are 8.4 and 2.5, respectively, for $10 \times 10 \times 1.6$ mm^3 dimension in two consecutive frequencies of 3.57 GHz and 11.67 GHz. The EMR value of 8.4 improves its homogeneity and reduces its electrical size without any fabrication limits.This benefit is accomplished by reducing the cost of coupling to the external field as shown by the minimum transmission value (−15 dB).

$$EMR = \frac{\lambda}{L} \tag{26}$$

The comparison between the proposed GCHSRR unit cell and the existing metamaterial unit cell is presented in Table 8. This is noticeable as compared to others; the unit cell has a high EMR as well as the proposed GCHSRR unit cell also covers the low frequency and high-frequency bands.

IX. CONCLUSION

Experimental and numerical demonstration of the negative index metamaterial unit cell and its array structure have been designed, simulated, measured, and analyzed in this paper. The proposed compact metamaterial unit cell consists of gap couple three hexagonal split ring resonators with electrical dimension of $0.119\lambda \times 0.119\lambda$ at 3.56 GHz. The double negative region has been found for the proposed metamaterial from 7.92 GHz to 9.78 GHz where the effective negative refractive index regions are from 6.30 GHz to 10.22 GHz and 11.97 GHz to 12.61 GHz that makes the propagation reversed where the radiations get bent backward to its structure and allows it to be applicable for different microwave applications. The effective absorption peaks are 99%, 98%, and 81% for 4.27 GHz, 5.42 GHz, and 12.40 GHz, respectively. To identify the effective parameters such as permittivity, permeability and refractive index, single and double negative characteristics, parametric studies have been carried out in terms of different lengths and different structures. The designed metamaterial exhibits single and double negative characteristics at S-band and X-band respectively which is later carried out for analysis and fabrication. The proposed GCHSRR unit cell and its 18 × 20 array structure have been fabricated and measured through the waveguide ports and reference horn antennas where the simulated and measured results have a good agreement between them. In addition, the scattering parameters have also been extracted from the circuit analysis by using ADS EM simulator software. The EMR values of the unit cell 8.4 specifies the compactness and acceptability, which reports that these designs are flexible in the practical microwave frequency band application with high absorptance. Therefore, the proposed designed metamaterial can be a prominent solution for many applications in microwave regions like navigation beacons, optical communications, wireless network, satellite communications, radar and space communications, etc.

REFERENCES

[1] A. R. Davoyan and N. Engheta, "Nonreciprocal emission in magnetized epsilon-near-zero metamaterials," *ACS Photon.*, vol. 6, no. 3, pp. 581–586, Mar. 2019.

[2] S. Yves, T. Berthelot, M. Fink, G. Lerosey, and F. Lemoult, "Left-handed band in an electromagnetic metamaterial induced by sub-wavelength multiple scattering," *Appl. Phys. Lett.*, vol. 114, no. 11, Mar. 2019, Art. no. 111101.

[3] N. Misran, M. T. Islam, M. Y. Ismail, and S. H. Yusop, "Analisis pencirian parameter ketebalan dan kebertelusan substrat bagi elemen cincin segiempat sepusat bersela antena tatasusun pantulan," *J. Kejuruter.*, vol. 23, pp. 11–15, Nov. 2011.

[4] M. R. Islam, M. Samsuzzaman, N. Misran, G. K. Beng, and M. T. Islam, "A tri-band left-handed meta-atom enabled designed with high effective medium ratio for microwave based applications," *Results Phys.*, vol. 17, Jun. 2020, Art. no. 103032.

[5] K. Srinivasan, N. B. Ali, Y. Trabelsi, M. S. M. Rajan, and M. Kanzari, "Design of a modified single-negative metamaterial structure for sensing application," *Optik*, vol. 180, pp. 924–931, Feb. 2019.

[6] N. Ramanujam, K. J. Wilson, P. Mahalakshmi, and S. A. Taya, "Analysis of photonic band gap in photonic crystal with epsilon negative and double negative materials," *Optik*, vol. 183, pp. 203–210, Apr. 2019.

[7] D. R. Smith, S. Schultz, P. Markoš, and C. M. Soukoulis, "Determination of effective permittivity and permeability of metamaterials from reflection and transmission coefficients," *Phys. Rev. B, Condens. Matter*, vol. 65, no. 19, pp. 1–5, Apr. 2002.
[8] F. S. Jafari, M. Naderi, A. Hatami, and F. B. Zarrabi, "Microwave Jerusalem cross absorber by metamaterial split ring resonator load to obtain polarization independence with triple band application," *AEU-Int. J. Electron. Commun.*, vol. 101, pp. 138–144, Mar. 2019.
[9] F. B. Ashraf, T. Alam, S. Kibria, and M. T. Islam, "A compact meander line elliptic split ring resonator based metamaterial for electromagnetic shielding," *Mater. Express*, vol. 8, no. 2, pp. 133–140, Apr. 2018.
[10] M. M. Hasan, M. R. I. Faruque, and M. T. Islam, "A tri-band microwave perfect metamaterial absorber," *Microw. Opt. Technol. Lett.*, vol. 59, no. 9, pp. 2302–2307, Sep. 2017.
[11] S. Ghosh and K. V. Srivastava, "An equivalent circuit model of FSS-based metamaterial absorber using coupled line theory," *IEEE Antennas Wireless Propag. Lett.*, vol. 14, pp. 511–514, 2015.
[12] H. Yuan, B. O. Zhu, and Y. Feng, "A frequency and bandwidth tunable metamaterial absorber in x-band," *J. Appl. Phys.*, vol. 117, no. 17, May 2015, Art. no. 173103.
[13] C.-Y. Wang, J.-G. Liang, T. Cai, H.-P. Li, W.-Y. Ji, Q. Zhang, and C.-W. Zhang, "High-performance and ultra-broadband metamaterial absorber based on mixed absorption mechanisms," *IEEE Access*, vol. 7, pp. 57259–57266, 2019.
[14] H. Zhai, C. Zhan, Z. Li, and C. Liang, "A triple-band ultrathin metamaterial absorber with wide-angle and polarization stability," *IEEE Antennas Wireless Propag. Lett.*, vol. 14, pp. 241–244, 2015.
[15] S. Khan and T. F. Eibert, "A multifunctional metamaterial-based dual-band isotropic frequency-selective surface," *IEEE Trans. Antennas Propag.*, vol. 66, no. 8, pp. 4042–4051, Aug. 2018.
[16] C. Sabah and T. Nesimoglu, "Design and characterization of a resonator-based metamaterial and its sensor application using microstrip technology," *Opt. Eng.*, vol. 55, no. 2, Feb. 2016, Art. no. 027107.
[17] M. J. Hossain, M. R. I. Faruque, and M. T. Islam, "Design and analysis of a new composite double negative metamaterial for multi-band communication," *Current Appl. Phys.*, vol. 17, no. 7, pp. 931–939, Jul. 2017.
[18] J. B. Pendry, A. J. Holden, D. J. Robbins, and W. J. Stewart, "Magnetism from conductors and enhanced nonlinear phenomena," *IEEE Trans. Microw. Theory Techn.*, vol. 47, no. 11, pp. 2075–2084, Nov. 1999.
[19] R. Marques, F. Mesa, J. Martel, and F. Medina, "Comparative analysis of edge- and broadside-coupled split ring resonators for metamaterial design–theory and experiments," *IEEE Trans. Antennas Propag.*, vol. 51, no. 10, pp. 2572–2581, Oct. 2003.
[20] R. Marqués, F. Medina, and R. Rafii-El-Idrissi, "Role of bianisotropy in negative permeability and left-handed metamaterials," *Phys. Rev. B, Condens. Matter*, vol. 65, no. 14, pp. 1–6, Apr. 2002.
[21] S. I. Maslovski, P. M. T. Ikonen, I. Kolmakov, S. A. Tretyakov, and M. Kaunisto, "Artificial magnetic materials based on the new magnetic particle: Metasolenoid," *Prog. Electromagn. Res.*, vol. 54, pp. 61–81, 2005.
[22] L. Yousefi and O. M. Ramahi, "Artificial magnetic materials using fractal Hilbert curves," *IEEE Trans. Antennas Propag.*, vol. 58, no. 8, pp. 2614–2622, Aug. 2010.
[23] J. D. Baena, R. Marqués, F. Medina, and J. Martel, "Artificial magnetic metamaterial design by using spiral resonators," *Phys. Rev. B, Condens. Matter*, vol. 69, no. 1, pp. 1–5, Jan. 2004.
[24] O. Luukkonen, S. I. Maslovski, and S. A. Tretyakov, "A stepwise nicolson–Ross–weir-based material parameter extraction method," *IEEE Antennas Wireless Propag. Lett.*, vol. 10, pp. 1295–1298, 2011.
[25] A. Hoque, M. T. Islam, A. Almutairi, T. Alam, M. J. Singh, and N. Amin, "A polarization independent quasi-TEM metamaterial absorber for x and ku band sensing applications," *Sensors*, vol. 18, no. 12, p. 4209, 2018.
[26] H. Cao, M. Shan, T. Chen, J. Lei, L. Yang, and X. Tan, "Triple-band polarization-independent ultrathin metamaterial absorber," *Prog. Electromagn. Res. M*, vol. 77, pp. 93–102, 2019.
[27] S. Ji, C. Jiang, J. Zhao, X. Zhang, and Q. He, "Design of a polarization-insensitive triple-band metamaterial absorber," *Opt. Commun.*, vol. 432, pp. 65–70, Feb. 2019.
[28] A. K. Singh, M. P. Abegaonkar, and S. K. Koul, "A triple band polarization insensitive ultrathin metamaterial absorber for S-C-and X-bands," *Prog. Electromagn. Res. M*, vol. 77, pp. 187–194, Dec. 2019.
[29] A. S. Dhillon, D. Mittal, and R. Bargota, "Triple band ultrathin polarization insensitive metamaterial absorber for defense, explosive detection and airborne radar applications," *Microw. Opt. Technol. Lett.*, vol. 61, no. 1, pp. 89–95, Jan. 2019.
[30] X. Zeng, M. Gao, L. Zhang, G. Wan, and B. Hu, "Design of a triple-band metamaterial absorber using equivalent circuit model and interference theory," *Microw. Opt. Technol. Lett.*, vol. 60, no. 7, pp. 1676–1681, Jul. 2018.
[31] S. R. Thummaluru, N. Mishra, and R. K. Chaudhary, "Design and analysis of an ultrathin triple-band polarization independent metamaterial absorber," *AEU-Int. J. Electron. Commun.*, vol. 82, pp. 508–515, Dec. 2017.
[32] D. Singh and V. M. Srivastava, "Triple band regular decagon shaped metamaterial absorber for X-band applications," in *Proc. Int. Conf. Comput. Commun. Informat. (ICCCI)*, vol. 1, Jan. 2017, pp. 5–8.
[33] A. F. Almutairi, M. S. Islam, M. Samsuzzaman, M. T. Islam, N. Misran, and M. T. Islam, "A complementary split ring resonator based metamaterial with effective medium ratio for C-band microwave applications," *Results Phys.*, vol. 15, Dec. 2019, Art. no. 102675.
[34] M. Hasan, M. Faruque, S. Islam, and M. Islam, "A new compact double-negative miniaturized metamaterial for wideband operation," *Materials*, vol. 9, no. 10, p. 830, 2016.
[35] T. M. Hossain, M. F. Jamlos, M. A. Jamlos, P. J. Soh, M. I. Islam, and R. Khan, "Modified H-shaped DNG metamaterial for multiband microwave application," *Appl. Phys. A, Solids Surf.*, vol. 124, no. 2, p. 183, Feb. 2018.
[36] Z. Zhou and H. Yang, "Triple-band asymmetric transmission of linear polarization with deformed S-shape bilayer chiral metamaterial," *Appl. Phys. A, Solids Surf.*, vol. 119, no. 1, pp. 115–119, Apr. 2015.
[37] M. M. Hasan, M. R. I. Faruque, and M. T. Islam, "Parametric studies on split S-shaped composite meta atom for X-band communication," *Bull. Polish Acad. Sci. Tech. Sci.*, vol. 65, no. 4, pp. 533–539, Aug. 2017.
[38] P. Liu, S. Yang, A. Jain, Q. Wang, H. Jiang, J. Song, T. Koschny, C. M. Soukoulis, and L. Dong, "Tunable meta-atom using liquid metal embedded in stretchable polymer," *J. Appl. Phys.*, vol. 118, no. 1, Jul. 2015, Art. no. 014504.
[39] S.-H. Liu, L.-X. Guo, and J.-C. Li, "Left-handed metamaterials based on only modified circular electric resonators," *J. Modern Opt.*, vol. 63, no. 21, pp. 2220–2225, Nov. 2016.

MOHAMMAD SHAHIDUL ISLAM (Student Member, IEEE) was born in Brahmanbaria, Bangladesh, in 1993. He received the B.Tech. degree (Hons.) in software engineering from Infrastructure University Kuala Lumpur, in 2018. He is currently pursuing the M.Sc. degree in electrical and electronic engineering with Universiti Kebangsaan Malaysia (UKM), Malaysia. He is also a Graduate Research Assistant with the Department of Electrical, Electronic, and Systems Engineering, UKM. He has authored or coauthored a number of refereed journals and conference papers. His research interests include the Internet of Things, antenna and wave propagation, wireless communication, and metamaterials.

MD. SAMSUZZAMAN (Member, IEEE) was born in Jhenaidah, Bangladesh, in 1982. He received the B.Sc. and M.Sc. degrees in computer science and engineering from Islamic University Kushtia, Bangladesh, in 2005 and 2007, respectively, and the Ph.D. degree from Universiti Kebangsaan Malaysia, Malaysia, in 2015. From 2008 to 2011, he was a Lecturer with the Patuakhali Science and Technology University (PSTU), Bangladesh, where he was an Assistant Professor with the Patuakhali Science and Technology University, from 2011 to 2015. He is currently an Associate Professor with PSTU. He is also a Postdoctoral Fellow with Universiti Kebangsaan Malaysia. He has authored or coauthored over 80 research journal articles, nearly 20 conference articles, and a few book chapters on various topics related to antennas, microwaves, and electromagnetic radiation analysis with one inventory patents filed. His Google scholar citation is 546 and H-index is 13. His research interests include communication antenna design, satellite antennas, and microwave imaging.

GAN KOK BENG was born in Malaysia, in 1978. He received the B.S. degree in material physics from University Technology Malaysia, in 2001. He has worked as an Optical-Design Engineer, from 2003 to 2005. He is currently an Associate Professor with the Centre of Advanced Electronic and Communication Engineering (PAKET), Universiti Kebangsaan Malaysia. His research interests include embedded system in healthcare and biomechanics and human motion analysis.

NORBAHIAH MISRAN received the B.Eng. degree in electrical, electronic, and system engineering from Universiti Kebangsaan Malaysia (UKM), in 1999, and the Ph.D. degree from the Queen's University of Belfast, Northern Ireland, U.K., in 2004. She started her career as a Tutor, in 1999. She later has been appointed as a Lecturer, in 2004, and an Associate Professor, in 2009. She is currently a Professor at UKM. Her research interests include RF device design, particularly in broadband microstrip antennas, reconfigurable antennas, and reflect array antennas. She is also conducting some researches in engineering education field.

NOWSHAD AMIN is currently serving as a Strategic Hire Professor with the Institute of Sustainable Energy of the National Energy University, Universiti Tenaga Nasional, Malaysia, as well as an adjunct to the Faculty of Engineering and Built Environment, Universiti Kebangsaan Malaysia (UKM). Earlier, he has served over 11 years at the Department of Electrical, Electronic and Systems Engineering, National University of Malaysia, Universiti Kebangsaan Malaysia, from November 2006 to January 2018, where he led the Solar Photovoltaic Research Group under the Solar Energy Research Institute (SERI).

MOHAMMAD TARIQUL ISLAM (Senior Member, IEEE) is currently a Professor with the Department of Electrical, Electronic, and Systems Engineering, Universiti Kebangsaan Malaysia (UKM), and a Visiting Professor of the Kyushu Institute of Technology, Japan. He is the author and coauthor of about 500 research journal articles, nearly 175 conference articles, and a few book chapters on various topics related to antennas, microwaves, and electromagnetic radiation analysis with 18 inventory patents filed. Thus far, his publications have been cited 5656 times and his H-index is 38 (Source: Scopus). His Google scholar citation is 7854 and H-index is 42. His research interests include communication antenna design, radio astronomy antennas, satellite antennas, and electromagnetic radiation analysis.

Dr. Islam received several International Gold Medal awards, a Best Invention in Telecommunication Award, a Special Award from Vietnam for his research and innovation, and Best Researcher Awards at UKM, in 2010 and 2011, respectively. He is a recipient of the 2018 IEEE AP/MTT/EMC Excellent Award. He also won the Best Innovation Award, in 2011, and the Best Research Group in ICT niche by UKM, in 2014. He was a recipient of the Publication Award from Malaysian Space Agency, in 2014, 2013, 2010, and 2009, respectively, and the Best Paper Presentation Award in 2012 International Symposium on Antennas and Propagation (ISAP 2012) at Nagoya, Japan, and in IconSpace, in 2015. He is a recipient of more than 40 research grants from the Malaysian Ministry of Science, Technology and Innovation, Ministry of Education, UKM Research Grant, and International Research Grants from Japan and Saudi Arabia. He is a Chartered Professional Engineer-CEng, a member of the IET (U.K.), and a Senior Member of IEICE, Japan. He currently serves as the Guest Editor for *SENSORS Journal*, and an Associate Editor for IEEE Access and *IET Electronics Letter*.